Enhanced modulation bandwidth of nanocavity light emitting devices

Erwin K. Lau[1*], Amit Lakhani[1], Rodney S. Tucker[2], and Ming C. Wu[1]

[1]Department of Electrical Engineering and Computer Sciences, University of California, Berkeley, Berkeley, California 94720
[2]ARC Special Research Centre for Ultra-Broadband Information Networks, Department of Electrical and Electronic Engineering, University of Melbourne, Vic 3010, Australia
[*]Corresponding author: elau@eecs.berkeley.edu

Abstract: We show that the direct modulation bandwidth of nano-cavity light emitting devices (nLEDs) can greatly exceed that of any laser. By performing a detailed analysis, we show that the modulation bandwidth can be increased by the Purcell effect, but that this enhancement occurs only when the device is biased below the lasing threshold. The maximum bandwidth is shown to be inversely proportional to the square root of the modal volume, with sub-wavelength cavities necessary to exceed conventional laser speeds.

©2009 Optical Society of America

References and links

1. R. S. Tucker, "High-speed modulation of semiconductor lasers," J. Lightwave Technol. **3**, 1180-1192 (1985).
2. E. M. Purcell, "Spontaneous emission probabilities at radio frequencies," Phys. Rev. **69**, 681 (1946).
3. Z. Zhang, L. Yang, V. Liu, T. Hong, K. Vahala, and A. Scherer, "Visible submicron microdisk lasers," Appl. Phys. Lett. **90**, 111119 (2007).
4. T. Baba, P. Fujita, A. Sakai, M. Kihara, and R. Watanabe, "Lasing characteristics of GaInAsP-InP strained quantum-well microdisk injection lasers with diameter of 2-10 μm," IEEE Photon. Technol. Lett. **9**, 878-880 (1997).
5. O. Painter, R. K. Lee, A. Scherer, A. Yariv, J. D. O'Brien, P. D. Dapkus, and I. Kim, "Two-Dimensional Photonic Band-Gap Defect Mode Laser," Science **284**, 1819-1821 (1999).
6. K. Nozaki, S. Kita, and T. Baba, "Room temperature continuous wave operation and controlled spontaneous emission in ultrasmall photonic crystal nanolaser," Opt. Express **15**, 7506-7514 (2007).
7. S.-W. Chang, C.-Y. A. Ni, and S.-L. Chuang, "Theory for bowtie plasmonic nanolasers," Opt. Express **16**, 10580-10595 (2008).
8. E. Feigenbaum and M. Orenstein, "Optical 3D cavity modes below the diffraction-limit using slow-wave surface-plasmon-polaritons," Opt. Express **15**, 2607-2612 (2007).
9. S. A. Maier and H. A. Atwater, "Plasmonics: Localization and guiding of electromagnetic energy in metal/dielectric structures," J. Appl. Phys. **98**, 011101-011110 (2005).
10. H. T. Miyazaki and Y. Kurokawa, "Squeezing Visible Light Waves into a 3-nm-Thick and 55-nm-Long Plasmon Cavity," Phys. Rev. Lett. **96**, 097401-097404 (2006).
11. T. Baba, "Photonic crystals and microdisk cavities based on GaInAsP-InP system," IEEE J. Sel. Top. Quantum Electron. **3**, 808-830 (1997).
12. E. Yablonovitch, (manuscript in progress).
13. J. M. Gérard and B. Gayral, "Strong Purcell effect for InAs quantum boxes in three-dimensional solid-state microcavities," J. Lightwave Technol. **17**, 2089-2095 (1999).
14. L. A. Coldren and S. W. Corzine, *Diode Lasers and Photonic Integrated Circuits* (John Wiley & Sons, Inc., New York, 1995), p. 143.
15. G. Björk and Y. Yamamoto, "Analysis of semiconductor microcavity lasers using rate equations," IEEE J. Quantum Electron. **27**, 2386-2396 (1991).
16. E. Yablonovitch, "Light Emission in Photonic Crystal Micro-Cavities," in *Confined Electrons and Photons: New Physics and Applications*, E. Burstein and C. Weisbuch, eds. (Plenum Press, New York, 1994), pp. 635-646.
17. M. Yamada and H. I. a. H. Nagato, "Estimation of the Intra-Band Relaxation Time in Undoped AlGaAs Injection Laser," Jpn. J. Appl. Phys. **19**, 135-142 (1980).
18. M. Asada, "Intraband relaxation time in quantum-well lasers," IEEE J. Quantum Electron. **25**, 2019-2026 (1989).

19. A. K. Sarychev and G. Tartakovsky, "Magnetic plasmonic metamaterials in actively pumped host medium and plasmonic nanolaser," Phys. Rev. B **75**, 085436-085439 (2007).
20. N. I. Zheludev, S. L. Prosvirnin, N. Papasimakis, and V. A. Fedotov, "Lasing spaser," Nat. Photon. **2**, 351-354 (2008).
21. M. T. Hill, Y. S. Oei, B. Smalbrugge, Y. Zhu, T. De Vries, P. J. Van Veldhoven, F. W. M. Van Otten, T. J. Eijkemans, J. P. Turkiewicz, H. De Waardt, E. J. Geluk, S. H. Kwon, Y. H. Lee, R. Notzel, and M. K. Smit, "Lasing in metallic-coated nanocavities," Nat. Photon. **1**, 589-594 (2007).
22. H. Yokoyama and S. D. Brorson, "Rate equation analysis of microcavity lasers," J. Appl. Phys. **66**, 4801-4805 (1989).
23. H. Altug, D. Englund, and J. Vučković, "Ultrafast photonic crystal nanocavity laser," Nat. Phys. **2**, 484-488 (2006).
24. Y. Arakawa, T. Sogawa, M. Nishioka, M. Tanaka, and H. Sakaki, "Picosecond pulse generation (< 1.8 ps) in a quantum well laser by a gain switching method," Appl. Phys. Lett. **51**, 1295-1297 (1987).
25. J. R. Karin, L. G. Melcer, R. Nagarajan, J. E. Bowers, S. W. Corzine, P. A. Morton, R. S. Geels, and L. A. Coldren, "Generation of picosecond pulses with a gain-switched GaAs surface-emitting laser," Appl. Phys. Lett. **57**, 963-965 (1990).
26. D. Hisamoto, W.-C. Lee, J. Kedzierski, H. Takeuchi, K. Asano, C. Kuo, E. Anderson, T.-J. King, J. Bokor, and C. Hu, "FinFET-a self-aligned double-gate MOSFET scalable to 20 nm," IEEE Trans. Electron. Dev. **47**, 2320-2325 (2000).
27. S. A. Backer, I. Suez, Z. M. Fresco, J. M. J. Frechet, J. A. Conway, S. Vedantam, H. Lee, and E. Yablonovitch, "Evaluation of new materials for plasmonic imaging lithography at 476 nm using near field scanning optical microscopy," Journal of Vacuum Science & Technology B: Microelectronics and Nanometer Structures **25**, 1336-1339 (2007).
28. R. Coccioli, M. Boroditsky, K. W. Kim, Y. Rahmat-Samii, and E. Yablonovitch, "Smallest possible electromagnetic mode volume in a dielectric cavity," Optoelectronics, IEE Proceedings - **145**, 391-397 (1998).
29. J.-P. Berenger, "Three-Dimensional Perfectly Matched Layer for the Absorption of Electromagnetic Waves," J. Comput. Phys. **127**, 363-379 (1996).
30. E. D. Palik, *Handbook of Optical Constants of Solids* (Academic Press, New York, 1998), pp. 350-357.

1. Introduction

Semiconductor nanocavities are of interest for their potential as threshold-less lasers and high-speed modulated sources. Typical light-emitting devices (LEDs) rely on the spontaneous emission (SpE) of a gain material as the primary light source (Fig. 1(a)). The modulation speed of such a device is limited by the rate of SpE in the bulk material: usually < 1 GHz. A laser places this gain material into a cavity, thus allowing optical feedback and a build-up of photons (Fig. 1(b)). This allows stimulated emission (StE) to dominate. Hence, the modulation speed of lasers is determined by the rate of StE, whose ultimate speed has been found to be limited by gain compression [1], on the order of 10's of GHz. The nanocavity light-emitting device (nLED) is an optical gain material placed in a sub-wavelength cavity (Fig 1c). It utilizes the small cavity size to enhance the rate of spontaneous emission [2], allowing faster modulation speeds than typical LEDs. The nLED differs from a nanocavity laser in that the cavity is designed specifically for enhanced spontaneous emission, rather than stimulated emission. In this respect, a much lower cavity quality factor (Q) can be implemented, since cavity losses need not be compensated by gain. In a conventional laser, SpE is typically much smaller than StE. By confining the gain in a nano-scale cavity, the Purcell-enhanced spontaneous emission rate can exceed the stimulated emission rate and potentially enable modulation speeds greatly surpassing that of any, including nanocavity, semiconductor lasers.
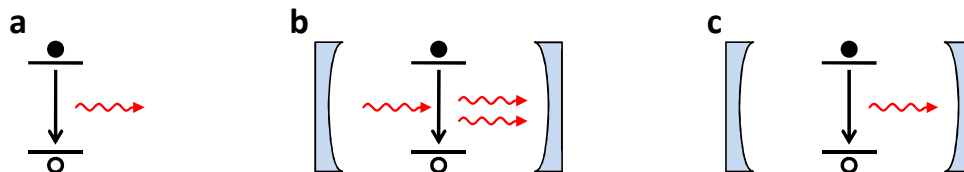

Fig. 1. Conceptual diagram of different optical emitters: (a) LED (b) laser (c) cavity-enhanced LED.

E.M. Purcell showed that the rate of spontaneous emission in a cavity can be enhanced by a factor F, which is proportional to Q/V_n [2]:

$$F = \frac{6}{\pi^2} \frac{Q}{V_n} ,$$ (1)

where V_n is the effective modal volume (V_{eff}) in units of cubic half-wavelengths: $V_n = V_{eff} /(\lambda_0/2n)^3$, where λ_0 is the modal wavelength, and n is the effective index of the cavity mode. Hence, a large Q and small modal volume are desired for large SpE rates. However, an extremely high Q will increase the photon lifetime, leading to slow photon decay times and poor modulation speeds. Therefore, in order to increase the SpE rate to surpass the StE rate typically found in high-speed lasers, a balance must be struck between SpE and photon decay times: moderate Q's (< 1000) and modal volumes much less than a cubic half-wavelength are necessary. Current optical cavity designs, such as microdisks [3, 4] and photonic crystals [5, 6], however, cannot achieve cavity volumes below a half-wavelength in each dimension. For example, the smallest demonstrated photonic crystal cavity volume [6] is $V_n = 1.2$. Fortunately, sub-wavelength volumes may be possible by designing plasmonic cavities whose operating frequency lies close to the plasmon resonance [7-10]. Hence, the plasmonic effect enables optical cavities that can potentially achieve SpE rates faster than the StE rates of nanocavity and conventional lasers alike.

This paper is structured as follows: first, the generalized rate equations are introduced. To provide more physical intuition, we derive the approximate bandwidth of nLEDs. Then, a more rigorous bandwidth derivation, which encompasses both LEDs and lasers, is given. Device design is optimized for bandwidth, showing that sub-wavelength cavities and sub-threshold conditions are necessary to achieve very high bandwidths. Finally, we introduce a potential design for a nano-plasmonic cavity, which illustrates the practical advantages and disadvantages of the nLED.

2. Rate equations

In order to characterize the modulation frequency response of the nLED, the dynamic rate equations are studied. In the most general case, both above- and below-threshold conditions (i.e. cavity-enhanced LEDs and lasers) can be described by the standard laser rate equations, with the addition of Purcell enhancement [11]:

$$\frac{dN}{dt} = J - GS - F\beta \frac{N}{\tau_{sp0}} - (1-\beta)\frac{N}{\tau_{sp0}} - \frac{N}{\tau_{nr}}$$ (2)

$$\frac{dS}{dt} = \left[\Gamma G - \frac{1}{\tau_p}\right]S + \Gamma F\beta \frac{N}{\tau_{sp0}} ,$$ (3)

where N and S are the carrier and photon densities, J is the pump current, G is the net StE gain, τ_{sp0} is the bulk spontaneous emission lifetime, τ_{nr} is the non-radiative lifetime, β is the fraction of spontaneous emission that couples to the fundamental optical mode, and Γ is the modal confinement factor.

3. Nano-cavity LED bandwidth

The nLED is designed to operate below threshold and its dynamics will be dominated by SpE. Therefore, the StE contribution can be ignored, allowing us to model the nLED as a LED in a cavity. Formally, this results in ignoring the StE terms in Eqs. (2) and (3), as well as the non-radiative term. We assume the cavity volume is smaller than $V_n = 1$ and the Q is sufficiently high, thus $F \gg 1$. Since the cavity volume is small, the free spectral range of the mode spacing will allow only one mode to overlap with the gain bandwidth, thus $\beta \approx 1$. This allows us to ignore the term signifying SpE into other modes (3rd term, right-hand side of Eq. (2)). The modulation frequency response can then be found by taking the small-signal

approximation of Eqs. (2) and (3). The response will be dominated by two first-order poles from the 1) enhanced spontaneous emission rate and 2) photon decay rate. The small-signal frequency response $H(\omega)$ will be

$$H(\omega) \equiv \frac{\Delta S(\omega)}{\Delta J(\omega)} = \frac{\Gamma}{\tau_p} \frac{1}{\left(1 + \dfrac{j\omega}{\gamma_p}\right)\left(1 + \dfrac{j\omega}{\gamma_{sp}}\right)}, \qquad (4)$$

where H is defined as the change in photon density ΔS per change in current ΔJ, γ_p is the photon decay rate, $\gamma_{sp} = F\beta/\tau_{sp0}$ is the enhanced modal SpE rate, and $\tau_{sp} = 1/\gamma_{sp}$ is the Purcell-reduced modal SpE lifetime. To find the 3-dB bandwidth, we find the frequency at which $|H(\omega)|^2$ is half the DC response. This yields a 3-dB bandwidth of

$$f_{3dB,\max} \approx \frac{1}{2\pi} \frac{1}{\sqrt{\tau_p^2 + \tau_{sp}^2}}. \qquad (5)$$

where $\tau_p = 1/\gamma_p = Q/\omega_0$ is the photon lifetime, ω_0 is the optical cavity frequency, τ_{sp0} is the bulk SpE lifetime, and β is the fraction of SpE that couples to the main optical mode. The bandwidths for a wide range of nLEDs with different Qs and volumes are shown in Fig. 2(a). Note that the photon lifetime τ_p and Purcell-reduced spontaneous emission lifetime τ_{sp} are proportional and inversely-proportional to Q, respectively. Hence, increasing cavity Q will enhance the spontaneous emission rate (via the Purcell effect), but the photons will remain in the cavity for a longer time. Hence Q must be optimized to achieve the highest bandwidth for a given modal volume. The optimal Q can be found by solving $d(f_{3dB,\max})/dQ = 0$. This optimal Q occurs when the photon and SpE lifetimes are equal:

$$Q_{opt} = \sqrt{\frac{\pi^2 \tau_{sp0} \omega_0 V_n}{6}}, \qquad (6)$$

where $\beta \approx 1$ for $V_n < 1$. By replacing τ_p and τ_{sp} in Eq. (5) to show their explicit Q-dependence and inserting Eq. (6), we see that the optimal bandwidth is proportional to $V_n^{-1/2}$:
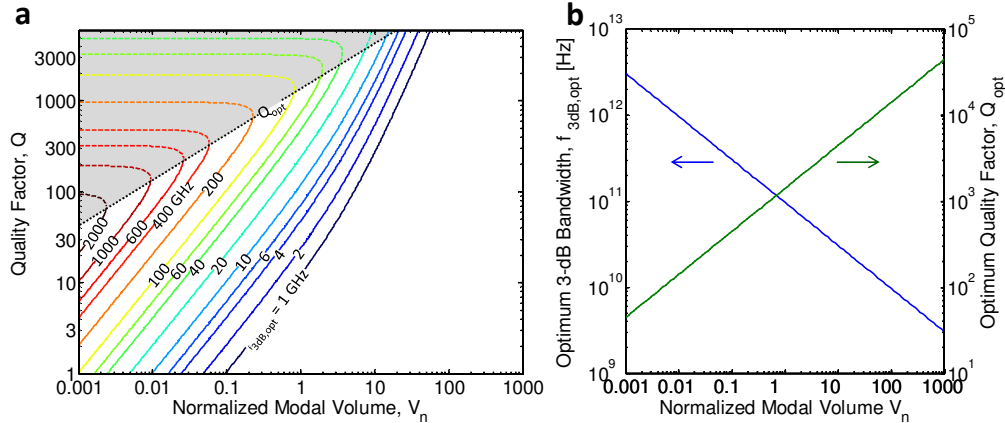

Fig. 2. (a) Contour plot of optimal 3-dB bandwidth for various nLED cavities with different modal volumes and quality factors. Bandwidth enhancement is found for small modal volumes, where there is a high Purcell enhancement. The dotted line (Q_{opt}) separates devices dominated by strong (above dotted line) and weak (below dotted line) coupling regimes. The strong-coupling regime is shaded, as it demonstrates richer dynamics and cannot be simply described by bandwidth. (b) Optimum 3-dB bandwidth and Q versus cavity volume.

$$f_{3dB,opt} \approx \frac{1}{2\pi}\sqrt{\frac{3\omega_0}{\pi^2 \tau_{sp0} V_n}} \; . \tag{7}$$

Both Q_{opt} and $f_{3dB,opt}$ are plotted in Fig. 2(b). This optimal bandwidth can be shown to be similar to the result when derived from an alternate approach [12]. The optimal Q is shown as the dotted line in Fig. 2(a), and is the contour where the cavity bandwidth equals the Purcell-enhanced SpE rate. This can also be interpreted as the border between regimes of strong and weak coupling [13]. The strong coupling regime ($Q > Q_{opt}$, dashed contours) will exhibit Rabi oscillations that decay at the photon lifetime, and may be of interest for quantum information processing. The weak coupling regime ($Q < Q_{opt}$, solid contours), due to lower cavity Q, allows for faster emission of photons and is attractive for high-speed optical communications. Hence, high-speed nLEDs must foremost be designed with small modal volumes to achieve enhanced SpE rates. Then, an appropriate Q must be chosen to allow the photons to decay from the cavity. Since the nLED is not required to lase, small Q's are acceptable, thus allowing very high cavity bandwidths.

4. Generalized 3-dB bandwidth

As shown in Fig. 2, cavity volume and Q are important parameters in the optimization of a light source for bandwidth. In addition to sub-threshold conditions, however, a thorough analysis must also consider above-threshold conditions (i.e. lasers). The rate equations shown in Eqs. (2) and (3) encompass the dynamics of both lasers and LEDs. In this section, we derive the 3-dB bandwidth from these rate equations, which will be general to Purcell- and non-Purcell-enhanced devices, biased above and below threshold. A small-signal linearization of the full dynamic equations in Eqs. (2) and (3) is performed [1, 14], yielding a modulation frequency response of

$$H(\omega) = \frac{\Gamma(aS_0 + \gamma_{sp})}{\omega_R^2 - \omega^2 + j\gamma\omega} \; . \tag{8}$$

This is a classical damped oscillator, whose resonance frequency, ω_R is

$$\omega_R^2 = \frac{1}{\tau_p}(aS_0 + \gamma_{sp}) + \frac{\Gamma}{\tau_{\Delta N}}\left(a_p S_0 + \gamma_{sp}\frac{N_0}{S_0}\right) \tag{9}$$

and damping, γ, equals

$$\gamma = aS_0\left(1 + \frac{\Gamma a_p}{a}\right) + \gamma_{sp} + \gamma_p - \Gamma G \; , \tag{10}$$

where a is the differential gain ($\equiv \partial G/\partial N$), a_p is the differential gain compression ($\equiv \partial G/\partial S$), and the subscript "0" denotes steady-state values. The 3-dB bandwidth (f_{3dB}) can be analytically calculated from the resonance frequency and damping [1, 14]:

$$f_{3dB} = \frac{1}{2\pi}\sqrt{\omega_R^2 - \frac{1}{2}\gamma^2 + \sqrt{\left(\omega_R^2 - \frac{1}{2}\gamma^2\right)^2 + \omega_R^4}} \; . \tag{11}$$

For the nLED-dominant approximation (SpE > StE), the resonance frequency and damping reduce to $\omega_R^2 \approx \gamma_{sp}\gamma_p$ and $\gamma \approx \gamma_{sp} + \gamma_p$, and the bandwidth reduces to Eq. (5).

The gain model used in these calculations was assumed to be a logarithmic fit to a quantum well active layer:

$$G = g_0 \ln\left(\frac{N + N_s}{N_{tr} + N_s}\right), \tag{12}$$

where g_0 is the gain coefficient, N_s is the linearity parameter [14], and N_{tr} is the transparency carrier density. However, the theory is general to any gain medium: quantum dot, quantum dash, quantum well, or bulk. The differential gains are defined as

$$a \equiv \frac{\partial G}{\partial N} = \frac{1}{1+\varepsilon S}\frac{g_0}{N+N_s} \text{ and } a_p \equiv -\frac{\partial G}{\partial S} = \frac{\varepsilon G}{1+\varepsilon S}. \qquad (13, 14)$$

The gain compression term εS results from ultra-fast intraband effects. Although gain compression has significant effect on the modulation response, it is less significant in the steady-state solutions, and is neglected when solving for the steady-state values of gain (i.e. $\varepsilon S_0 = 0$, but $a_p \neq 0$). The previous literature [11, 15] failed to include gain compression in their rate equation analysis. This led to conclusions that showed above-threshold lasers eventually reached modulation bandwidths equal to the cavity bandwidth, $\Delta\omega = Q/\omega_0$, which greatly overestimates the bandwidth. β can be approximated as the ratio of the optical mode bandwidth to the total spontaneous emission bandwidth [16]: $\beta = 1/(1 + \pi \cdot \Delta\lambda \cdot V_n/\lambda_0)$, where $\Delta\lambda$ is the bandwidth of SpE in the gain medium. The parameters used in this paper are: $g_0 = 1.1$ s^{-1}, $N_s = 0.11 \times 10^{18}$ cm^{-3}, $N_{tr} = 1.2 \times 10^{18}$ cm^{-3}, $\Gamma = 0.1$, $\lambda_0 = 1550$ nm, $\varepsilon = 1.5 \times 10^{-17}$ cm^3, $\tau_{sp0} = 1$ ns, $\tau_{nr} = 1$ ns, $n = 3.5$, and $\Delta\lambda = 80$ nm.

5. Generalized analysis and device optimization

In this section, we show that the bandwidth of a lasing nanocavity is essentially the same as conventional lasers, regardless of Purcell enhancement. Furthermore, we postulate that nLEDs with Purcell-enhanced spontaneous emission can potentially achieve much higher bandwidths than lasers. This is shown by numerically computing the 3-dB bandwidth of the generalized light emitting device, taking in account StE and SpE. The analytic results in Section 4 are evaluated for a representative Purcell-enhanced nanocavity with $V_n = 0.2$ and $Q = 400$ at a modal wavelength of 1.55 µm. Fig. 3(a) illustrates the direct modulation frequency response as the pump bias is increased from below threshold to above threshold. One should first note that, unlike conventional lasers, the modulation response at any bias is highly damped, with no observable resonance peak. More importantly, however, Fig. 3(a) shows that as the laser pump bias is increased, the 3-dB modulation bandwidth *decreases*. This trend is opposite that of a classical laser whose highest bandwidth bias is well-above threshold. In fact, the highest bandwidth in this example (190 GHz) occurs at a bias level *below* threshold, where SpE dominates.

This non-intuitive result is explained by comparing the StE and SpE rates. A light-emitting device can be considered lasing when the output light is predominantly coherent. In other words, the StE rate must be much larger than the SpE rate in the cavity. This occurs as the pump rises well above the transition point J_1 (defined as the pump current where StE and SpE rates are equal, shown in Fig. 3(b)). This condition is valid even in nanocavity lasers, where the SpE rate can be large, and can be used to define laser threshold [15]. Well above threshold, the modulation response is dominated by the StE dynamics. Although the resonance frequency at this point is enhanced by StE (Fig. 3(c)), the damping factor increases at a faster rate (Fig. 3(d)), causing the bandwidth to decrease (Fig. 3(e)). As bias is further increased, the bandwidth approaches the well-known classical result, which is primarily reduced by the gain compression of StE in the laser [1]. This typically limits the bandwidth of all lasers to several factors below the cavity bandwidth (f_0/Q), typically less than 50 GHz. However, when the LED is biased below lasing, where SpE is dominant, the cavity dynamics are determined only by the SpE rate and cavity bandwidth. In this case, the bandwidth can well exceed 100 GHz (Fig. 3(e)). In a LED, gain compression is not a dominant effect, since SpE is not, to first-order, a function of the photon density. Thus, in order to maximize bandwidth, a sub-threshold device is desired.

To optimize 3-dB bandwidth, a mapping of the maximum bandwidth for different cavity designs, including LEDs and lasers, is plotted in Fig. 3(f). Devices with different cavity volumes and Qs are simulated. For each device, the bias is swept through both below- and

above-threshold pump current levels, and the largest bandwidth value is plotted. The devices categorized as classical lasers lie in the upper right of the dashed boundary (labeled "Conventional Lasers"), where $V_n > 10$ and the Purcell factor is weak (and Q is sufficiently high to achieve lasing). These devices are characterized as having an optimal bandwidth when biased above threshold, where StE dominates. However, this lasing bandwidth is limited to, at most, ~ 50 GHz. The remaining parameter space, labeled "LED", designate devices whose maximum bandwidth occurs at sub-threshold pump levels, where SpE dominates. Within this regime, the Purcell-dominant devices are those with $V_n < 1$. Here, StE can be neglected and the dynamics are governed mainly by the SpE rate and photon lifetime, and the bandwidth can be approximated by Eq. (5). Although this basic theory projects bandwidths in excess of 1 THz, other carrier dynamics, such as intracavity scattering lifetimes [17, 18] (~ 100 fs) or electron transit times, will ultimately limit the speed of modulation.

Currently, much research has been focused on the attempt to create a nano-plasmonic cavity laser [7, 19-21]. Although the modulation response enhancement of Purcell-enhanced LEDs has not previously been explored, it is important to acknowledge that several groups have studied the enhancement of laser dynamics via the Purcell effect, proposing nanocavity lasers with bandwidths over 100 GHz [11, 15, 22, 23]. However, the theoretical works failed
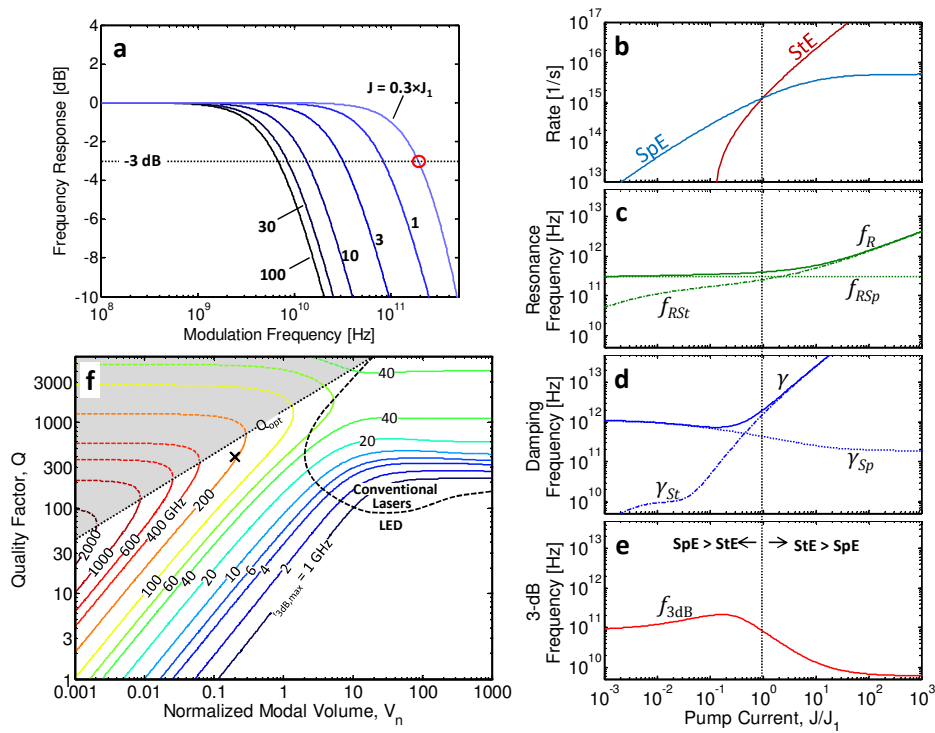

Fig. 3. (a) Normalized frequency response as a function of different pump currents for a Purcell-enhanced nanocavity light emitter with $Q = 400$ and $V_n = 0.2$. The largest 3-dB bandwidth (red circle) occurs *below* threshold and is $f_{3dB,max} \approx 200$ GHz. When biased above threshold, the bandwidth decreases to 6 GHz. (b) Spontaneous emission (SpE) and stimulated emission (StE) rates versus pump current (normalized to J_1). For currents below the dotted line, the SpE rate is greater than the StE rate. This is reversed above J_1. (c) Resonance frequency (f_R) and (d) damping rate (γ) versus current. In (c) and (d), the contributions from SpE and StE are separately shown using a "Sp" and "St" subscript, respectively. (e) 3-dB bandwidth (f_{3dB}) versus current. When StE dominates, the bandwidth drops due to increased damping from gain compression. (f) Contour plot of maximum 3-dB bandwidth for nanocavity-emitters (including both lasers and LEDs) with different modal volumes and quality factors. The dashed contour separates the devices where the maximum bandwidth is found below or above J_1, labeled "LED" and "Conventional Lasers", respectively. The strong-coupling regime is similarly labeled with a dotted line as in Fig. 2. The "x" marks the example device in panel (a) through (e).

to include gain compression, thus overestimating the maximum lasing bandwidth as equal to the cavity bandwidth. The experimental work attempts to demonstrate this enhancement by presenting optical pump-probe pulses from 2-D photonic crystal lasers [23], but their results suffer from a few shortcomings. Optical pump-probe using short pump pulses has been known to generate short optical pulses through gain switching, and the pulse width cannot be used as a direct measure of laser bandwidth. Optical pulses comparable to or shorter than those reported in [23] have been reported in optically gain-switched conventional semiconductor lasers whose bandwidths are well below 50 GHz [24, 25]. Additionally, the calculated SpE rate from their experiments ($\tau_{sp} = \tau_{sp0}/F \geq 8.4$ ps) signify any contribution of the Purcell-enhanced SpE to the pulse width must be eclipsed by StE, indicating that these are essentially conventional lasers. Finally, the record bandwidth was calculated using the inverse cavity lifetime $1/\tau_p$, which ignores both a factor of 2π reduction and gain compression effects that practically limit the laser bandwidth to well-below the cavity bandwidth [1].

6. Nano-LED design

In order to achieve sufficiently high SpE enhancement, sub-wavelength cavity volumes must be utilized. Currently, the most promising technology for achieving such cavities is by utilizing surface plasmon modes [7-10]. One possible nLED cavity design is presented to illustrate the advantages of designing ultra-small sub-wavelength cavities. Shown in Fig. 4a, The device geometry resembles that of a Fin-FET (field-effect transistor) [26], which may reduce processing and growth complexity [19]. A P-I-N junction is covered by a 2 nm thick passivation layer. The P and N metal contacts are removed for clarity. A silver layer is deposited on top of the passivation layer, over the intrinsic region, which also contains the active gain material. The plasmonic cavity, therefore, extends only the length (*L*) of the silver layer. In order to increase radiation resistance for efficient out-coupling, the metal stripe can be extended along the substrate (perpendicular to *L*) without greatly affecting the cavity mode. The surrounding metal simultaneously achieves sub-wavelength confinement, a straightforward method for electrical injection, and facilitated thermal conduction for enhanced heat dissipation. The coupling of the metal to the optical mode naturally reduces the cavity-*Q* in the form of Ohmic losses, making the device unsuitable for laser operation. However, from Fig. 3(f), a cavity volume of $V_n = 0.01$ only needs $Q > 10$ in order to achieve bandwidths above 100 GHz. Quantum efficiency (see Appendix) may be kept high by engineering a high output radiation rate. The high radiation rate and Ohmic losses can be afforded since the nLED need not reach threshold to operate. Two different sub-wavelength cavity dimensions are simulated in Fig. 4. The device in Fig. 4(b), with dimensions $W \times H \times L = 20 \times 40 \times 140$ nm^3, shows a simulated cavity mode with a resonance at 1500 nm, $V_n = 0.0015$, $Q = 10$, and a quantum efficiency of $\eta = 40\%$ (where we assumed 100% conversion of carriers to photons). An additional design with dimensions $W \times H \times L = 20 \times 20 \times 50$ nm^3 is shown in Fig. 4(c). The cavity resonance is 1600 nm, $V_n = 0.007$, $Q = 11$, and a quantum efficiency of $\eta = 55\%$. The calculated 3-dB bandwidths, based on the cavity volume and Q, of these two structures are 660 GHz and 160 GHz, respectively. It is important to note that these bandwidth calculations assume that the perfect alignment of the dipole emitter to the optical mode's polarization, maximum field intensity, and center frequency [13]. Practical engineering of the cavity and gain medium may potentially reduce this overlap, and careful optimization is important. It is also important to reiterate that this design is not unique; these results are general and may be applied to any nLED cavity design.

The small cavity volume and large optical mode-metal overlap of nano-plasmonic cavities will result in low cavity Q. For example, a bulk Q of 10-20 can be expected for gold or silver in the near-infrared [27]. The plasmonic nanocavity can expect to have similar non-radiative Qs. These low Q values are sufficient for the nLED, since the radiative rate can be engineered to be comparable to the non-radiative photon decay rate, yielding quantum efficiencies similar to lasers. Indeed, a short photon lifetime is preferred, as it will increase the cavity bandwidth, as shown by Eq. (5). The small cavity volumes are offset by a short photon lifetime and high quantum efficiencies, so output powers > 100 μW range can be

obtained, which is sufficient for many applications, such as optical interconnects. The small volumes of the nLED provide an inherent benefit of greatly reduced current and power consumption. Additionally, the nLED bandwidth is enhanced over a wide range of sub-threshold bias levels, as shown in Fig. 3(e). This has a two-fold benefit. First, current levels will be greatly reduced from lasers (including "thresholdless" lasers), which must waste additional power for StE to overcome SpE. Furthermore, since the bandwidth is enhanced over a wide range of pump levels (unlike a laser, which must be pumped hard to reach large bandwidths), large extinction ratios can be maintained at ultra-high speeds. This is attractive
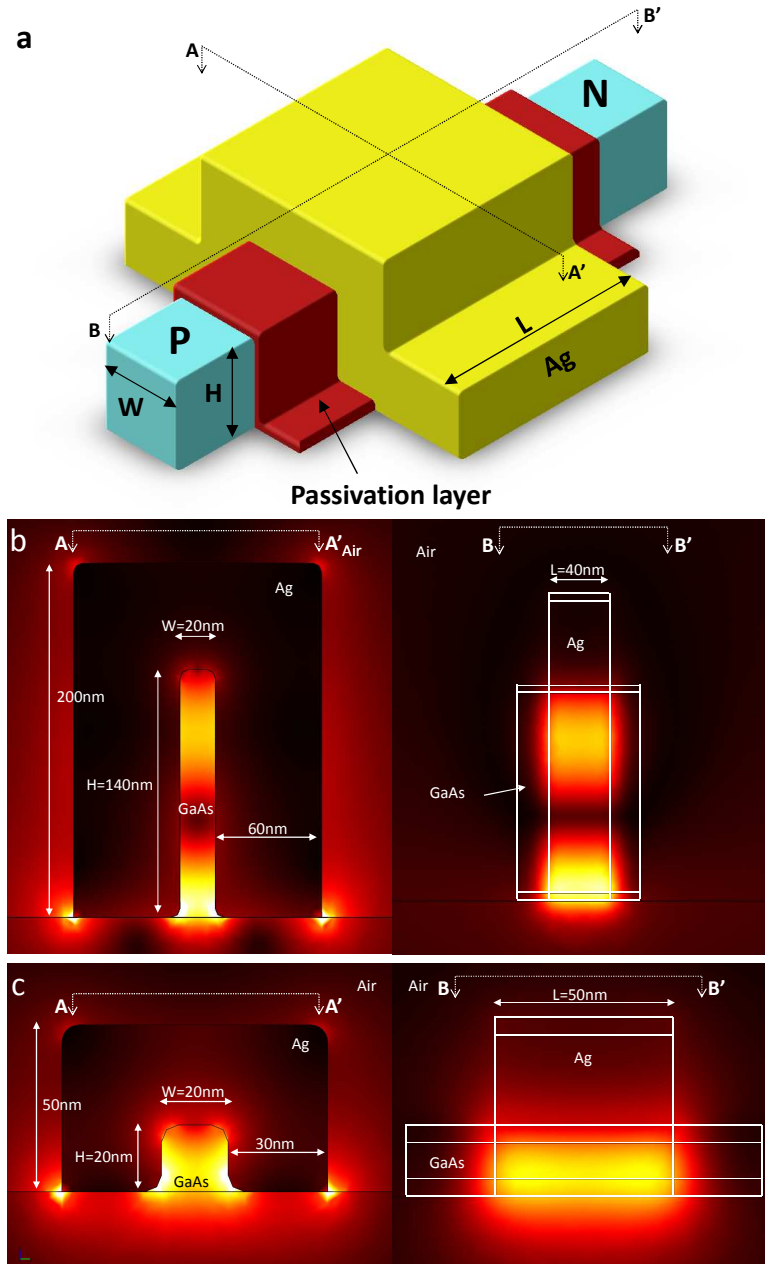

Fig. 4. (a) Schematic of proposed nLED structure. P and N are the ends of a P-I-N diode, where the intrinsic region is covered by the passivation layer and silver. Front and side cross-sections of the electric field magnitude profile for (b) $V_n = 0.007$ and (c) $V_n = 0.0015$.

for large-signal digital modulation applications. In addition, because of the small optical cavity, the SpE can be designed to couple to a single mode, making the linewidth distinctly different from (and potentially much smaller than) traditional LEDs. The single-mode linewidth will be primarily limited by the photon lifetime. However, since nLEDs are inherently based on spontaneous emission, the linewidth will also be enhanced by phase noise of the SpE.

7. Conclusion

The rate equations are analyzed to derive the bandwidth of nLEDs. Purcell-enhanced nLEDs are shown to potentially achieve modulation bandwidths much higher than conventional lasers. The bandwidth, shown in Eq. (5), is the inverse of the root-sum-square of the photon and Purcell-reduced spontaneous emission lifetimes. The optimal bandwidth is inversely proportional to the square root of the cavity modal volume. When Purcell-enhanced devices are biased above threshold, the bandwidth is shown to reduce due to gain compression, approaching that of conventional, non-Purcell-enhanced lasers. Hence, Purcell-enhanced bandwidths are optimally realized for sub-threshold devices. Sub-wavelength cavities are shown to be necessary to achieve extremely high bandwidths, achievable by utilizing plasmonics. Careful design of the cavity and emitter mode overlap is important to optimize the Purcell effect. At present, many considerations must be addressed for the realization of these devices. Nevertheless, nLEDs will be attractive for applications where coherence requirements are relaxed, such as intrachip or short-distance optical interconnects.

Appendix 1. Mode simulation

Mode profile, effective volume, cavity Q, and quantum efficiency were calculated using a commercial finite-element method solver, COMSOL. Each structure was solved in 3 dimensions, and the effective volume was integrated from the field density [28]. Cavity Q was calculated as $Q_{tot} = f/\Delta f$ by using a monochromatic quasi-plane wave excitation source and then finding the enhancement of energy versus wavelength inside the cavity. A perfectly matched layer (PML) was placed around the entire simulation to prevent unphysical reflections [29]. The dielectric constant of silver was obtained from experimental data [30]. Each tetrahedral mesh element had a maximum size of 4 nm inside the metal and dielectric cavity region. Quantum efficiency was defined as

$$\eta = \frac{1/\tau_{rad}}{1/\tau_{rad} + 1/\tau_{loss}} \, , \tag{15}$$

where the loss rate $1/\tau_{loss}$ (from the metal) was calculated through Poynting's theorem, and the radiation rate $1/\tau_{rad}$ was found by the relation

$$\frac{1}{Q_{tot}} = \frac{1}{Q_{rad}} + \frac{1}{Q_{loss}} \, . \tag{16}$$

Acknowledgments

The authors wish to thank Prof. Eli Yablonovitch for useful discussions.